POLITECNICO DI TORINO
Repository ISTITUZIONALE

Preliminary structural design of the IDEA Drift Chamber

Original
Preliminary structural design of the IDEA Drift Chamber / Corrado, M., Zavarise, G., Rawat, R., Grancagnolo, F.. - In: NUCLEAR PHYSICS. B. - ISSN 0550-3213. - ELETTRONICO. - 1033:(2026), pp. 1-11. [10.1016/j.nuclphysb.2026.117701]

Availability:
This version is available at: 11583/3015810 since: 2026-10-29T11:59:03Z

Publisher:
Elsevier

Published
DOI:10.1016/j.nuclphysb.2026.117701

Terms of use:

This article is made available under terms and conditions as specified in the corresponding bibliographic description in the repository

Publisher copyright

(Article begins on next page)

06 November 2026

Nucl. Phys. B 1033 (2026) 117701

Contents lists available at ScienceDirect

Nuclear Physics, Section B

journal homepage: www.elsevier.com/locate/nuclphysb

High Energy Physics – Phenomenology

Preliminary structural design of the IDEA drift chamber

Mauro Corrado [a,*], Giorgio Zavarise [a], Rakesh Rawat [a], Francesco Grancagnolo [b]

[a] Politecnico di Torino, Corso Duca degli Abruzzi, 24, Torino, 10129, Italy
[b] Istituto Nazionale di Fisica Nucleare Sezione di Lecce, Via Arnesano, Lecce, 73100, Italy

ARTICLE INFO

Editor: Pamela Ferrari

Keywords:
Particle detection
Drift chamber
Composite materials
Finite element analysis

ABSTRACT

The IDEA (Innovative Detector for Electron-positron Accelerator) drift chamber is a large, ultra-light gaseous tracking detector whose very low material budget is enabled by an innovative wire-support and assembly concept. Its large dimensions, combined with the requirements of low mass and high stiffness, pose significant challenges for structural design and material selection. This work presents a preliminary structural design of the wire cage, with particular emphasis on the endplates, which consist of an outer ring, an inner ring, radial spokes, and suspension cables supporting almost 340,000 anodic and cathodic wires. A hierarchical two-stage optimization strategy is adopted. In the first stage, Response Surface Methodology and Kriging surrogate models are used for geometric sizing, seeking a compromise between low structural mass, reduced spoke deformation, and adequate buckling resistance. In the second stage, a genetic algorithm is used to optimize the suspension-cable prestresses and further reduce spoke deflection. The optimized prestress distribution reduces the maximum spoke deflection from 24.34 mm to 0.564 mm. Although this value remains above the preliminary working target of 0.2 mm, the results demonstrate the effectiveness and structural feasibility of the cable-stayed endplate concept at the present preliminary-design stage. Further refinement will be required once the final composite material system and detector-level requirements have been defined.

1. Introduction

Particle detectors are among the most sophisticated and precise instruments used in experimental physics. They are designed to detect, track, and measure the properties of subatomic particles, including their energy, momentum and electric charge. Advances in nuclear and particle physics have therefore been closely linked to the development of increasingly accurate and efficient detector technologies.

Among gaseous tracking detectors, the drift chamber is widely used to reconstruct the trajectories of charged particles. The first studies of drift chambers date back to the work of Bressani, Charpak, Rahm and Zupančič in 1969, while the first functional drift chamber was developed by A.H. Walenta, Heintze and Schürlein in 1971 [1]. A schematic representation of the operating principle is shown in Figs. 1 and 2.

When a charged particle passes through the gas filling the chamber, it interacts electromagnetically with the atoms of the medium and produces electron-ion pairs along its trajectory. The electrical signal associated with the ionization produced by a single particle is, however, too small to be directly detected. For this reason, an intrinsic amplification mechanism is required.

An electric field is established inside the chamber by applying appropriate potentials to the anode and cathode electrodes. The electrons generated by ionization drift towards the positively charged anode wires. In most of the drift region, the electric field is

* Corresponding author.
E-mail address: mauro.corrado@polito.it (M. Corrado).

https://doi.org/10.1016/j.nuclphysb.2026.117701
Received 3 May 2026; Received in revised form 18 September 2026; Accepted 22 October 2026
Available online 24 October 2026
0550-3213/© 2026 The Authors. Published by Elsevier B.V. Funded by SCOAP[3]. This is an open access article under the CC BY license (http://creativecommons.org/licenses/by/4.0/).

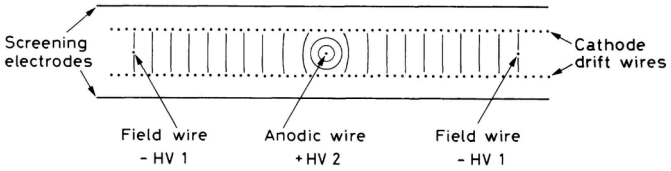


Fig. 1. Schematic of the drift chamber [5].

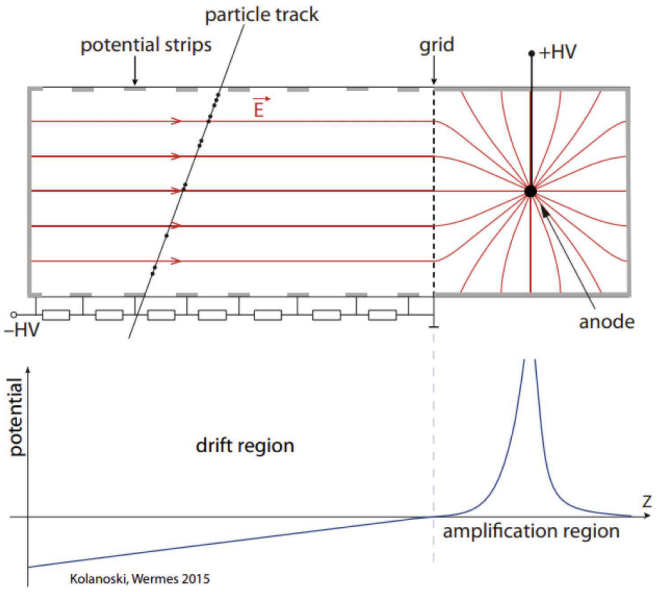


Fig. 2. Drift chamber working scheme.

sufficiently low that the electrons mainly undergo drift. Close to the thin anode wire, however, the electric field becomes much stronger because of the small wire radius. The electrons can consequently acquire sufficient energy between collisions to ionize additional gas molecules, producing an avalanche multiplication process. The resulting charge amplification generates a measurable electrical signal at the anode. To obtain sufficiently high electric fields and gas amplification, very thin anode wires, typically with diameters of the order of 20–100 μm, are used (Fig. 2). The statistical nature of the electron-gas interactions can be characterized by the mean free path λ between ionizing collisions [2].

The electrons produced along the particle trajectory drift towards the anode with a velocity that depends on the gas composition and the applied electric field, and this dependence is generally nonlinear in gaseous detectors [3]. By measuring the time interval between the passage of the particle and the arrival of the electrons at the anode, the position at which the ionization occurred can be reconstructed. The drift displacement relative to the starting position can be expressed as:

$$\Delta x = \int_{t_{start}}^{t_{stop}} v_D(t)\, dt \tag{1}$$

where v_D is the electron drift velocity. The spatial resolution therefore depends primarily on the accuracy with which the electron drift time and the corresponding drift velocity are determined, rather than simply on the spacing between signal electrodes. It depends, therefore, on the gas mixture, electric-field configuration, cell geometry, and the method used to reconstruct the electron drift time. To reconstruct charged-particle trajectories over large detector volumes, many drift cells must be arranged together. Each cell contains a signal wire, or anode, surrounded by electrodes maintained at cathode potential. Depending on the detector geometry, these cells can be arranged in planar or cylindrical configurations [4]. Cylindrical drift chambers, such as the one schematically illustrated in Fig. 3, are particularly suitable for collider experiments because their axis can be aligned with the beam direction.

1.1. Initial concept of the IDEA drift chamber

Several drift chambers have been proposed or operated before the development of the IDEA (Innovative Detector for Electron-positron Accelerator) concept. Examples include KLOE at the Frascati Φ-factory DAΦNE, the CluCou Chamber proposed for the 4th Concept at ILC, the I-tracker proposed for the Mu2e experiment at Fermilab [6,7], and the drift chamber developed for the MEG-II upgrade at PSI [8,9].

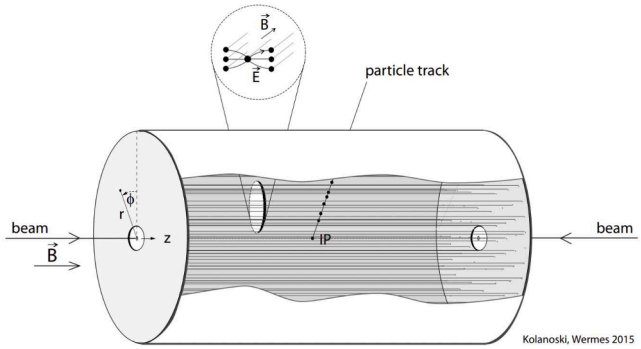


Fig. 3. Cylindrical drift chamber with cathode and anode wires parallel to magnetic field. The cut out shows the arrangement of drift cells.

IDEA is one of the detector concepts currently under development for experiments at future e^+e^- colliders, including FCC-ee. The current baseline configuration comprises a silicon pixel vertex detector, a large and lightweight central drift chamber, surrounding silicon micro-strip detectors, a thin superconducting solenoid, a μ-RWELL pre-shower detector, a dual-readout calorimeter, and a μ-RWELL muon system located within the magnet return yoke [10,11]. The detector concept and several of its subsystems are still undergoing development and optimization in the framework of the FCC-ee detector R&D programme. The IDEA drift chamber is conceived to provide efficient charged-particle tracking, high-precision momentum measurements, and particle identification through the cluster-counting technique [12]. For the IDEA drift chamber, a transverse single-cell spatial resolution of approximately $100\ \mu$m is currently considered in the detector design [13]. A key feature of the design is the very low amount of material traversed by particles, i.e. its high transparency in terms of radiation lengths.

The IDEA central drift chamber is a high-granularity, full-stereo and low-mass cylindrical detector operating inside a 2 T solenoidal magnetic field and filled with a helium-based gas mixture [14]. Its geometry was initially conceptualized by the Italian Istituto Nazionale di Fisica Nucleare (INFN) [13]. The chamber has an inner radius $R_{\text{in}} = 350$ mm, an outer radius $R_{\text{out}} = 2000$ mm, a total length of 4500 mm and an active length of 4000 mm. It consists of 112 coaxial wire layers, grouped into 14 super-layers of eight layers each, arranged in 24 identical azimuthal sectors with alternating-sign stereo angles. The tracking system contains 56,448 sense wires, 284,256 field wires and 2016 guard wires. The sense wires are 20 μm-diameter gold-plated molybdenum wires, whereas the field wires are 40 μm-diameter silver-plated aluminium wires and the guard wires are 50 μm-diameter silver-plated aluminium wires. The wires are arranged azimuthally in cells, each consisting of a sense wire surrounded by field wires. To maintain an approximately constant cell area of about 1.5 cm^2, the number of cells increases from the inner to the outer super-layers, from 192 cells at the innermost layer to 816 cells at the outermost one. The chamber geometry and wire arrangement therefore combine high granularity with a very large number of mechanically tensioned wires.

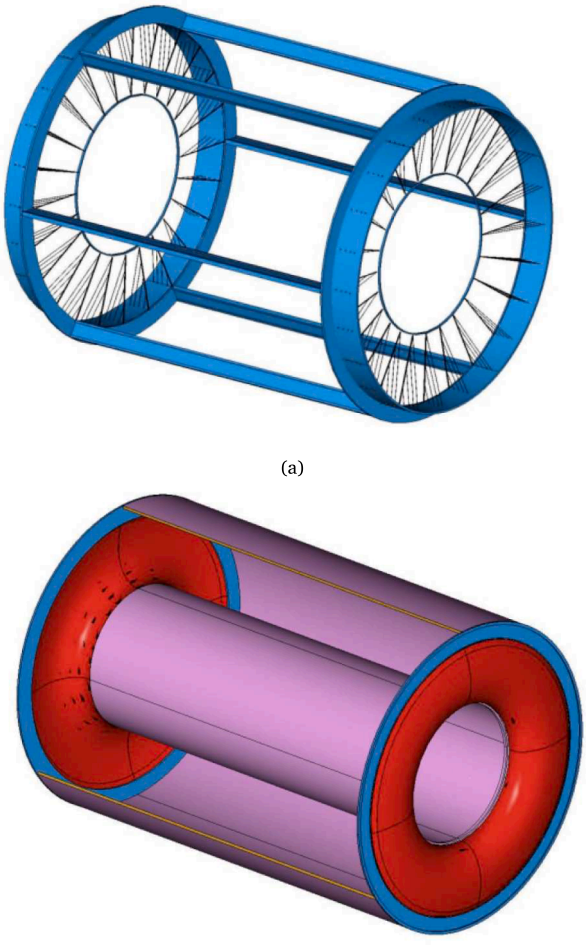
Such a large number of wires makes the mechanical support system a critical part of the detector design. At the same time, the amount of structural material must be minimized in order to preserve the transparency required for particle tracking. To reconcile these competing requirements, the functions of gas containment and wire support are separated in the IDEA concept. The wires are supported by an independent lightweight structure, referred to as the wire cage (Fig. 4a), whereas the gas mixture is contained by a thin external structure, referred to as the gas vessel (Fig. 4b). In this way, deformation of the gas vessel does not directly affect the position or mechanical tension of the internal wires.

The tension of the wires is transmitted to the endplates through a system of radial spokes extending between the inner and outer rings. Because the spokes must remain extremely lightweight while carrying substantial loads, they are supported by thin suspension cables, as shown schematically in Fig. 5. The resulting structural arrangement is analogous to a cable-stayed bridge: the outer ring plays a role similar to that of the tower, the spokes act as the deck, and the suspension cables provide additional stiffness. By appropriately tuning the forces in the cables, the transverse deformation of the spokes can be reduced. The spokes, suspension cables, inner ring and outer ring together constitute one endplate. Two such endplates are connected by a cylindrical carbon-fibre support structure that carries the overall system.

The IDEA drift chamber concept is therefore driven by the simultaneous need for accurate tracking, high granularity and extremely low material content. In particular, its design aims to:

- minimize the material contribution of the inner cylinder and endplates by separating the wire-support and gas-containment functions;
- adopt a feed-through-less wiring configuration,[1] allowing thinner wires to be used while increasing chamber granularity and the field-to-sense-wire ratio, thereby reducing both multiple scattering and the total wire load acting on the endplates;

[1] "Feed-through-less wiring" refers to a construction in which the wires are anchored to support boards mounted on the wire cage rather than being individually passed through feed-throughs in a gas-tight endplate. Spacers between adjacent spokes define the cell geometry, while the wire cage is mechanically separated from the gas vessel.



(a)

(b)

Fig. 4. Concept of the IDEA drift chamber: (a) lightweight wire cage support structure with feed-through-less wiring; (b) gas containment.

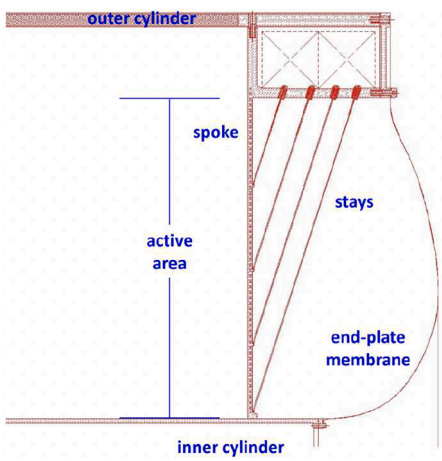


Fig. 5. Schematic showing connectivity of the stays, spokes, outer ring and inner ring.

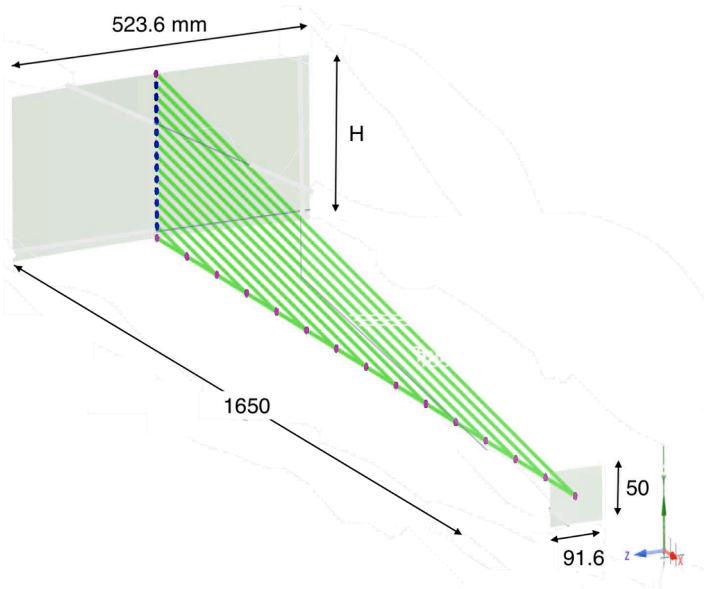


Fig. 6. Schematic of one of the cyclic symmetric sectors of the endplate analysed in the FE model.

- exploit cluster timing,[2] which can provide spatial resolutions below 100 μm for 8 mm drift cells in helium-based gas mixtures;
- exploit cluster counting for particle identification,[3] targeting a dN_c/dx resolution below 3%, approximately a factor of two better than conventional dE/dx measurements.

These characteristics impose particularly demanding requirements on the mechanical design of the wire cage. The structure must sustain the loads generated by the large number of tensioned wires while limiting deformation and, at the same time, introducing as little material as possible into the detector volume. The preliminary structural design of this system, with particular emphasis on the endplates, is the subject of the following sections.

2. Preliminary structural design of the wire cage

The present study concerns the preliminary design of the wire cage and, more specifically, of one of the endplate systems. The gas vessel is excluded from this study. Considering the circular periodicity of the geometry of the endplate, being made up in the initial configuration of 24 spokes with a sectoral angle of 15°, the analysis can be limited to one sector, imposing the proper symmetry boundary conditions. Each sector consists of a spoke 1650 mm long having rectangular cross section, an arch of the outer ring 523.6 mm long and an arch of the inner ring 91.6 mm long and 50 mm high (see Fig. 6). Each spoke is supported by 14 suspension cables. This number was selected during preliminary design studies as a compromise between deformation-control capability and geometric compactness of the endplate. Increasing the number of cables would provide a more distributed support system and additional freedom for prestress tuning; however, it would also require a larger number of attachment points and, consequently, a greater height of the outer ring. This would increase both the overall endplate envelope and its structural mass. Fourteen cables were therefore retained as a suitable balance between structural effectiveness and the lightweight, compact design requirements. All the other geometrical parameters, namely, height H and thickness T of the outer ring, thickness t of the inner ring, width b and height d of the spoke's cross section, and radius r of the suspension cables were not predefined, but were determined through an optimization process.

All numerical simulations were carried out in the ANSYS Workbench environment [15]. The geometry was created in SpaceClaim, while the static structural analyses were performed using ANSYS Mechanical. The ANSYS optiSLang environment was used to manage the Design of Experiments, surrogate model construction, and optimization workflow [16].

[2] "Cluster timing" refers to the use of the drift times of successive resolvable ionization clusters, rather than only the first detected cluster, to improve the estimate of the distance of closest approach between the track and the sense wire and, consequently, the spatial resolution of the cell.

[3] "Cluster counting" is a particle-identification technique based on the number of resolvable primary ionization clusters per unit track length, dN_{el}/dx. It exploits the approximately Poissonian statistics of primary ionization and counts clusters rather than integrating their charge, thereby reducing the large fluctuations affecting conventional dE/dx measurements.

2.1. Mechanical design requirements

The tracking performance of the drift chamber requires accurate and stable positioning of the sense wires. Since the IDEA drift chamber is designed to provide a transverse single-cell spatial resolution of the order of 100 μm [13], deformation of the wire-support system must be carefully controlled so that mechanical effects do not significantly degrade the detector performance.

The wires are very slender structural elements, with diameters of the order of 20–50 μm, and are therefore particularly sensitive to transverse deformation. Under their own weight, wires suspended between the two endplates develop a catenary-like sag. As an illustrative example, a 20 μm diameter molybdenum wire with a length of 4 m exhibits a mid-span sag of approximately 210 μm when tensioned with a load of about 0.3 N. Increasing the wire tension reduces this sag, but simultaneously increases the mechanical load carried by the wire and the risk of yielding or failure.

An additional contribution arises from electrostatic interactions between wires held at different electric potentials. In particular, the attractive forces between anodic and cathodic wires tend to reduce their separation and may further increase their transverse displacement. Sufficient wire pretension is therefore required both to limit gravitational sag and to maintain the stability of the wire configuration under electrostatic loading.

These requirements result in a substantial load acting on the endplates. The IDEA drift chamber contains approximately 340,000 wires, each pretensioned with a load of 0.3 N, corresponding to a total resultant load of 100 kN. This load is transferred to the endplates through the radial spokes. Considering the distribution of the wires along the detector radius and the adopted number of spokes, the load acting on each spoke is approximated in the structural model as a linearly varying distributed load, increasing from 0 N/mm at the inner ring to 5.05 N/mm at the outer ring.

2.2. Base finite element model

The aim of the IDEA drift chamber project is to design an ultra-light drift chamber in fibre reinforced composite material, which is an orthotropic layered material. However, at this preliminary modelling stage, the inner ring, outer ring, and spokes were represented using an equivalent monolithic orthotropic material with the same effective elastic properties as the reference composite laminate. The reason for this material modelling approach is that the initial design is deformation based, aimed at defining the geometrical parameters of the main components in order to minimize the deformation of the spokes. Stresses and strains, whose distributions depend on the specific layered structure of the composite material, are checked in a later stage. Furthermore, performing the needed parametric studies and optimization using such a monolithic orthotropic material is much less time consuming than with a composite material. The elastic properties of the monolithic orthotropic material were determined by applying the classic laminate theory [17]. The reference composite material is made with epoxy resin and carbon fibres, all oriented in the 0° direction. The obtained equivalent properties are listed in Table 1.

The outer and inner rings were modelled using eight-node SHELL281 elements. The size of the shell elements was set equal to 1 mm, based on a mesh convergence analysis. The spokes were modelled using three-node nonlinear BEAM189 elements, whereas the suspension cables were represented by two-node LINK180 truss elements.

Besides the symmetry boundary conditions, the translation in the axial direction of the drift chamber (Y direction in Fig. 6) was constrained along the bottom edge of the outer ring, simulating the support provided by the structure connecting the two endplates.

Owing to the high flexibility of the structural components, particularly the spokes, geometric nonlinearities were included by performing large-displacement analyses. This formulation was also required to correctly represent the behaviour of the suspension cables.

2.3. Geometric sizing optimization

Preliminary analyses revealed excessive compressive forces in the spokes and a significant risk of buckling. The number of spokes was therefore increased from 24 to 36, and the cyclic sector geometry and the load assigned to each spoke were updated accordingly. With 36 spokes, the angular extent of the cyclic sector was reduced from 15° to 10°. Accordingly, the arc lengths of the outer and inner rings included in the sector were reduced from 523.6 mm to 349.1 mm and from 91.6 mm to 61.1 mm, respectively, while the spoke length remained unchanged at 1650 mm. Since the total load generated by the tensioned wires is distributed among a larger number of spokes, the linearly varying distributed load acting on each spoke was correspondingly reduced from 0–5.05 N/mm to 0–3.37 N/mm, increasing from the inner ring toward the outer ring. Then, the structural design of the endplate was carried out through a hierarchical two-stage optimization strategy. The first stage, described in the present section, is a geometric sizing optimization aimed at defining an efficient baseline configuration of the endplate. Six geometric parameters are varied in order to obtain a compromise between low structural mass and reduced spoke deformation, while preserving adequate buckling resistance. Since transparency and low material budget are key requirements of the drift chamber, structural mass is given greater importance at this stage than the achievement of the final displacement target. The purpose of this first optimization is therefore not to satisfy the final spoke-deflection target directly, but to identify a lightweight geometry with acceptable structural performance to be used as the basis for the subsequent prestress optimization. In the second stage, described in Section 4, the optimized geometry is kept fixed and the prestress values of the suspension cables are varied. This second optimization is specifically devoted to deformation control and aims at reducing the spoke displacement toward the preliminary detector-level target.

The ANSYS optiSLang environment was used to manage the optimization process. For each of the six design variables, a range of admissible values was defined, as reported in Table 2. The optimization workflow consisted of three main stages:

Table 1
Elastic properties of the monolithic orthotropic material equivalent to the composite material.

Material property	Value	
Young's modulus in X direction (parallel to fibres)	1.21×10^5	MPa
Young's modulus in Y and Z directions	8.6×10^3	MPa
Poisson's ratio XY	0.27	
Poisson's ratio YZ	0.40	
Poisson's ratio XZ	0.27	
Shear modulus XY	4.7×10^3	MPa
Shear modulus YZ	3.1×10^3	MPa
Shear modulus XZ	4.7×10^3	MPa
Density	1500	kg/m^3

Table 2
List of the input variable parameters with their defined range of variation and optimized value.

Parameter	Range of values (mm)	Optimized value (mm)
Height of the outer ring, H	90 – 400	200
Thickness of the outer ring, T	3 – 15	14.4
Thickness of the inner ring, t	3 – 15	10.0
Width of the spoke cross section, b	3 – 20	9.6
Height of the spoke cross section, d	3 – 20	16.6
Radius of the cables, r	0.25 – 2.5	1.5
Performance after optimization		
Maximum spoke deflection	21.64 mm	
Total mass (per sector)	2.63 kg	
Buckling load multiplier	2.21	

(a) Design of Experiments (DOE): a set of combinations of the six geometric input parameters was generated within the prescribed design ranges. In the present study, an Optimal Space-Filling Latin Hypercube Sampling strategy was adopted to obtain an efficient and approximately uniform exploration of the multidimensional design space. Latin Hypercube Sampling provides a stratified exploration of the multidimensional input space [18], while optimized space-filling variants improve the uniformity of the sample distribution over the design domain [19]. The Optimal Space-Filling implementation available in ANSYS optiSLang was adopted in the present study.
(b) Meta-model construction: the results of the finite-element simulations generated through the DOE were used to construct surrogate models relating the input parameters to the structural responses. Although different surrogate model techniques are available within optiSLang, in the present work a Kriging Response Surface (KRS) was adopted because of its suitability for representing nonlinear relationships between the design variables and the structural responses.
(c) Response-surface optimization: the resulting surrogate models were used to search the design space for a suitable compromise between structural mass and spoke deflection, with greater priority assigned to mass reduction in accordance with the low-material-budget requirement of the detector. The resulting candidate design was subsequently verified through the full finite-element model. At this stage, a further constraint was imposed on the buckling performance, requiring a nonlinear buckling load multiplier greater than 2.0. This value was adopted as a preliminary engineering safety target to ensure an adequate margin against instability, rather than as a criterion derived from a specific design standard.

The simulations were automated using a Python script in SpaceClaim for parametric geometry generation. Each component was assigned a named selection to enable automatic model updating. For each DOE sample, the geometry was regenerated and transferred to ANSYS Mechanical, where the static structural analysis was performed. The resulting spoke deflection and structural mass were then returned to optiSLang for surrogate model construction and optimization.

Because the number of possible combinations of the six design variables is very large, only a subset of the design space was evaluated through finite-element simulations according to the adopted DOE strategy. The generated dataset was then used to construct the surrogate models relating the design variables to the structural responses.

The Kriging Response Surface methodology was used to approximate the relationship between the six geometric design variables and the structural responses [20]. The resulting surrogate models provide rapid predictions throughout the explored design domain and were therefore used for the subsequent optimization. Since surrogate model predictions are approximate, the selected optimal design was finally re-evaluated using the full finite-element model.

The result of the optimization process is reported in Table 2. The relatively large spoke deflection obtained at this stage should be interpreted in the context of the hierarchical optimization strategy: the first stage is primarily intended to determine a lightweight geometry, whereas the further reduction of deformation is delegated to the cable-prestress optimization described in Section 4.

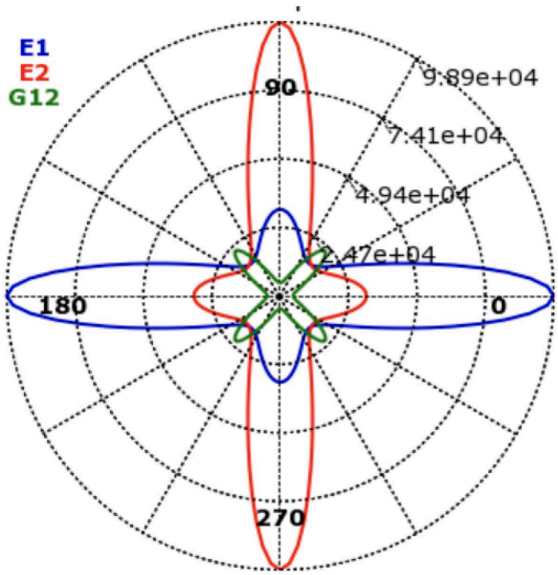


Fig. 7. Polar representation of the in-plane elastic properties of the [0/0/90/0/0] laminate. E_1 (blue) and E_2 (red) denote the Young's moduli along the local material directions 1 and 2, respectively, while G_{12} (green) denotes the in-plane shear modulus. Values are expressed in MPa. (For interpretation of the references to colour in this figure legend, the reader is referred to the web version of this article.)

3. Validation with composite material

The first stage of design was based on the assumption that using a monolithic equivalent orthotropic material would yield the same result as a true layered composite material. The validity of the equivalent-material assumption is assessed in this section by reanalyzing the optimized design using an explicit layered composite material made from epoxy resin and carbon fibres. For this design, a ply thickness of 0.2 mm was adopted. Five unidirectional plies were stacked according to the sequence [0/0/90/0/0], forming a 1-mm-thick laminate. This stacking sequence was selected to maximize the fraction of fibres oriented along the primary load-carrying direction of each component while providing sufficient transverse stiffness. The polar representation of the in-plane elastic properties of the [0/0/90/0/0] laminate is shown in Fig. 7. Here, E_1 and E_2 denote the Young's moduli along the local material directions 1 and 2, respectively, while G_{12} is the in-plane shear modulus. The directional variation of these quantities highlights the anisotropic stiffness of the laminate. For each component, a suitable number of 1-mm-thick laminate units was stacked to achieve the thickness obtained from the optimization process. (Table 2).

The ANSYS Composite PrepPost (ACP) tool was used to define the layered composite model. The maximum spoke deflection obtained with the layered composite model is 24.34 mm, slightly larger than the 21.64 mm obtained with the equivalent monolithic model. The deformed shape is shown in Fig. 8. This difference arises because the equivalent monolithic material used during the optimization corresponds to a fully unidirectional fibre-reinforced material, whereas the layered composite contains 80% of the fibres in the longitudinal direction and 20% in the transverse direction. The different mechanical behaviour of the two materials is evident by comparing the value of their Young's modulus in the 0° direction: 121,000 MPa for the fully unidirectional laminate (see Table 1) and 98,900 MPa for the bidirectional laminate (see Fig. 7).

4. Cable-prestress optimization

The optimization described in Section 2 represents the first stage of the hierarchical design strategy and is primarily devoted to geometric sizing. Once the lightweight endplate geometry was defined and subsequently verified using the layered composite model, the second optimization stage was performed by tuning the prestress of the suspension cables. Unlike the first stage, in which mass reduction plays a dominant role together with deformation and buckling performance, the objective of this second stage is specifically to minimize spoke deflection and approach the preliminary displacement target of approximately 0.2 mm. This value was suggested by the detector-physics collaborators on the basis of their experience and the anticipated wire-positioning needs; it does not represent a formal acceptance limit derived from a standard or from a finalized detector-level specification. The objective of the following optimization is therefore to quantify the effectiveness of cable prestressing and to determine how closely the present lightweight structural concept can approach this target.

The ultra-light structure is highly sensitive to the distribution of cable prestress. An inappropriate combination of prestress values may increase spoke deformation and reduce buckling resistance. Consequently, the prestresses of the 14 suspension cables were treated as independent design variables and optimized using a Genetic Algorithm (GA). Each cable prestress was constrained to the range 0–960 MPa. The GA was initialized with a population of 140 randomly generated individuals, while subsequent generations

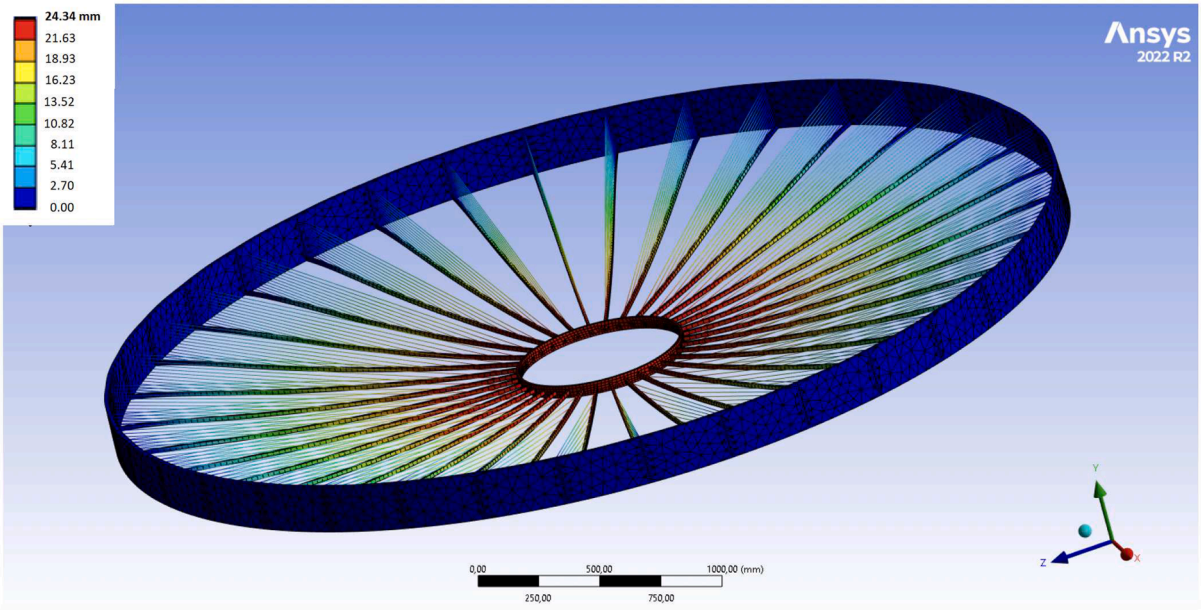


Fig. 8. Deformed shape of the endplate system made with fibre-polymer composite material subjected to a resultant load of 100 kN.

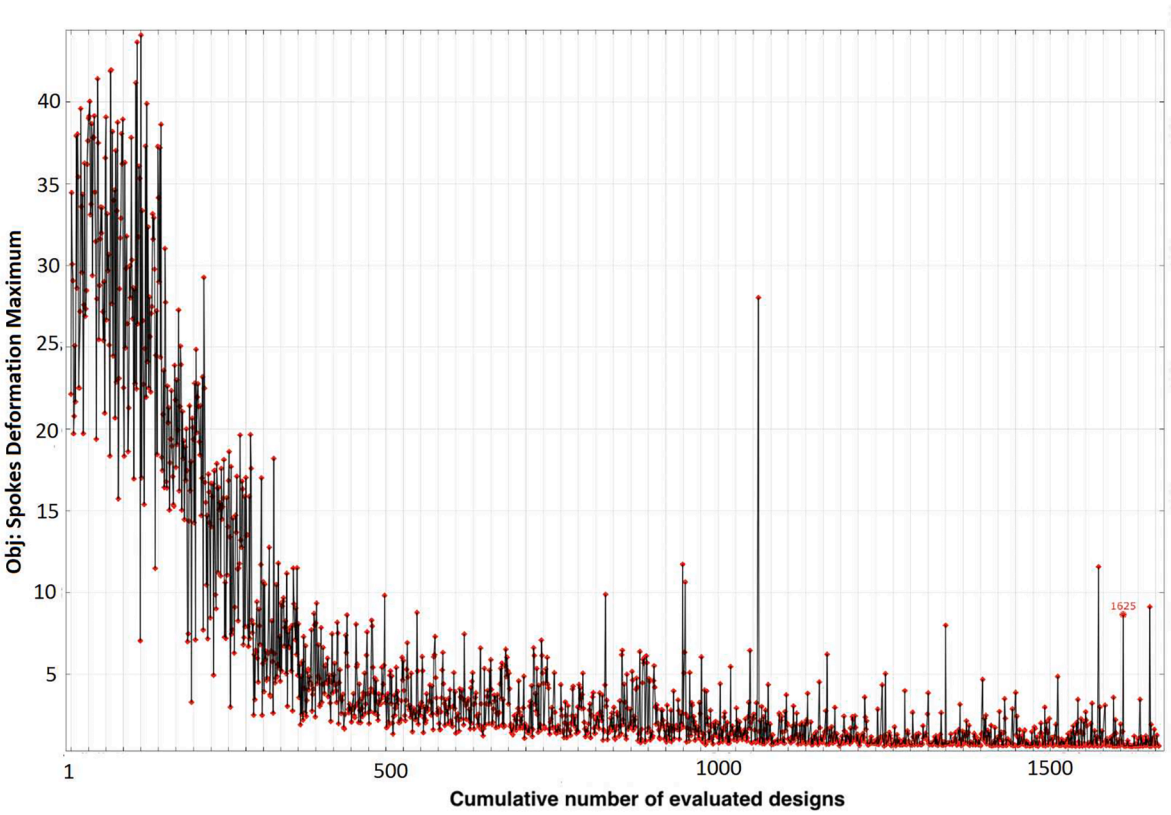


Fig. 9. Maximum spoke deflection during the GA optimization as a function of the cumulative number of evaluated candidate designs.

Table 3
Prestress in the cables obtained from optimization. Cable-1 is the outermost cable near the inner ring. Cable-14 is the innermost cable near the outer ring.

Cable no.	Prestress (MPa)
Cable-1	768
Cable-2	851
Cable-3	850
Cable-4	755
Cable-5	812
Cable-6	356
Cable-7	720
Cable-8	536
Cable-9	856
Cable-10	442
Cable-11	176
Cable-12	622
Cable-13	398
Cable-14	370

consisted of 70 individuals. A mutation probability of 7% was adopted. Fig. 9 shows the maximum spoke deflection obtained for the candidate designs evaluated during the GA optimization. The horizontal axis represents the cumulative number of evaluated candidate solutions rather than the generation number. The initial population consists of 140 randomly generated individuals, whereas each subsequent generation contains 70 individuals. During the first generations, the algorithm explores a broad region of the design space, resulting in a large scatter of the maximum spoke deflection. As the optimization progresses, the population increasingly concentrates in regions associated with lower deflection values. The improvement becomes progressively smaller, and no significant reduction of the best objective value was observed after approximately the 18th generation. The optimization was therefore terminated after the 24th generation.

The optimized prestress values for the fourteen cables are reported in Table 3. The corresponding average and maximum deflection in the spokes are 0.428 mm and 0.564 mm, respectively. The maximum value obtained does not satisfy the preliminary working target of 0.2 mm. Nevertheless, compared with the maximum deflection of 24.34 mm obtained for the unprestressed composite model, the optimized cable prestressing reduces the maximum deflection by approximately 97.7%, bringing the structural response into the sub-millimetre range. The present result should therefore be interpreted as a proof-of-feasibility and a preliminary design iteration, rather than as a detector-qualified final solution. Moreover, the current optimization varies only the prestress values of the fourteen suspension cables, while the structural geometry and representative material model are kept fixed. Consequently, the value of 0.564 mm should not be regarded as a lower bound for the final design. Further coupled optimization of the geometry, laminate configuration, and cable prestresses will be required after the final material system, construction details, and detector-level requirements have been defined.

5. Conclusions

The preliminary structural design of the IDEA drift-chamber wire cage was investigated, with particular emphasis on the endplate system. The design problem is especially challenging because the structure must withstand the loads generated by a very large number of tensioned wires while maintaining a very low material budget and limiting structural deformation.

A hierarchical two-stage optimization strategy was adopted. In the first stage, the main geometric parameters of the endplate were optimized to obtain a lightweight baseline configuration with reduced spoke deformation and adequate buckling resistance. To limit the computational cost of the design exploration, the initial optimization was performed using an equivalent monolithic orthotropic material, and the resulting configuration was subsequently re-evaluated using an explicit layered composite model. This comparison supported the suitability of the equivalent-material approach for preliminary geometric sizing, while also showing the influence of the actual laminate architecture on the structural stiffness.

In the second stage, the geometry was kept fixed and the prestress values of the fourteen suspension cables were optimized to further reduce the spoke deflection. The optimized prestress distribution reduced the maximum spoke deflection from 24.34 mm for the unprestressed composite model to 0.564 mm, corresponding to a reduction of approximately 97.7%. The resulting average spoke deflection was 0.428 mm. Although the maximum deflection remains above the preliminary working target of approximately 0.2 mm, the results demonstrate the effectiveness of the cable-stayed concept in controlling the deformation of an extremely lightweight endplate system.

The present configuration should therefore be regarded as a proof-of-feasibility and a preliminary structural-design iteration rather than as a final detector design. Further development will require the definition and experimental characterization of the actual

composite material system, including the fibre and resin systems, laminate architecture, manufacturing process, and connection details. Once these parameters and the final detector-level requirements have been established, the geometry, laminate configuration, and cable prestresses can be further refined through a coupled optimization procedure.

Declaration of competing interest

The authors declare that they have no known competing financial interests or personal relationships that could have appeared to influence the work reported in this paper.

Data availability

No data was used for the research described in the article.

References

[1] I.B. García Ferreira, J. García Herrera, L. Villaseñor, The drift chambers handbook, introductory laboratory course (based on, and adapted from, A H Walenta's course notes), J. Phys. Conf. Ser. 18 (1) (2005) 346. https://doi.org/10.1088/1742-6596/18/1/010
[2] W. Blum, W. Riegler, L. Rolandi, Particle Detection with Drift Chambers, Springer-Verlag Berlin Heidelberg, 2008.
[3] M. Alfonsi, G. Bencivenni, W. Bonivento, A. Cardini, P. de Simone, F. Murtas, D. Pinci, M.P. Lener, D. Raspino, B. Saitta, The triple-GEM detector for the M1R1 muon station at LHCb, in: IEEE Nuclear Science Symposium Conference Record, 2005, 2, 2005, pp. 811–815.
[4] H. Kolanoski, N. Wermes, Particle Detectors: Fundamentals and Applications, Oxford University Press, Oxford, 2020.
[5] W.R. Leo, Techniques for Nuclear and Particle Physics Experiments: A How-to Approach, Springer-Verlag Berlin Heidelberg, 1993.
[6] S. Miscetti, Mu2e Collaboration, Status of the Mu2e experiment, Nucl. Instrum. Methods Phys. Res. Sect. A 1073 (2025) 170257.
[7] L. De Lorenzis, F. Grancagnolo, A. L'Erario, A. Maffezzoli, A. Miccoli, S. Rella, M. Spedicato, G. Zavarise, Analysis and characterization of the mechanical structure for the I-tracker of the Mu2e experiment, Nucl. Phys. B (Proc. Suppl.) 248-250 (2014) 134–136.
[8] G.F. Tassielli, A.M. Baldini, G. Cavoto, F. Cei, M. Chiappini, G. Chiarello, A. Corvaglia, M. Francesconi, L. Galli, F. Grancagnolo, M. Grassi, M. Hildebrandt, M. Meucci, A. Miccoli, D. Nicolò, M. Panareo, A. Papa, F. Raffaelli, F. Renga, P. Schwendimann, G. Signorelli, C. Voena, The drift chamber of the MEG II experiment, J. Instrum. 15 (2020) C09051.
[9] R. Assiro, L. Cappelli, M. Cascella, L.D. Lorenzis, F. Grancagnolo, F. Ignatov, A. L'Erario, A. Maffezzoli, A. Miccoli, G. Onorato, M. Perillo, G. Piacentino, S. Rella, F. Rossetti, M. Spedicato, G. Tassielli, G. Zavarise, Ultra-low mass drift chambers, Nucl. Instrum. Methods Phys. Res. Sect. A 718 (2013) 443–445.
[10] W. Elmetenawee, G. Chiarello, A. Corvaglia, F. Cuna, N. De Filippis, E. Gorini, F. Grancagnolo, M. Maggi, A. Miccoli, M. Panareo, M. Primavera, G.F. Tassielli, A. Ventura, The tracking performance for the IDEA drift chamber, in: Proceedings of 41st International Conference on High Energy Physics — PoS(ICHEP2022), 414, 2022, p. 362. https://doi.org/10.22323/1.414.0362
[11] M. Dam, Detector requirements, design, and technologies for the FCC-ee Higgs, electroweak, and top factory, Nucl. Instrum. Methods Phys. Res. Sect. A 1080 (2025) 170648. https://doi.org/10.1016/j.nima.2025.170648
[12] G.F. Tassielli, A proposal of a drift chamber for the IDEA experiment for a future e^+e^- collider, in: Proceedings of 40th International Conference on High Energy Physics — PoS(ICHEP2020), 390, 2021, p. 877.
[13] M. Abbrescia, et al., (IDEA Study Group), The IDEA detector concept for FCC-ee (2025). arXiv:2502.21223 [physics.ins-det]
[14] F. Cuna, G. Chiarello, A. Corvaglia, N.D. Filippis, E. Gorini, F. Grancagnolo, A. Miccoli, M. Primavera, G.F. Tassielli, A. Ventura, A proposal of a He based drift chamber as central tracker for the IDEA detector concept for a future e^+e^- collider, in: Proceedings of the European Physical Society Conference on High Energy Physics — PoS(EPS-HEP2021), 398, 2022, p. 786. https://doi.org/10.22323/1.398.0786
[15] ANSYS, Inc., ANSYS Mechanical, Release 2025 R2, ANSYS, Inc., Canonsburg, PA, USA, 2025.
[16] ANSYS, Inc., optiSLang User's Guide, Release 2025 R2, ANSYS, Inc., Canonsburg, PA, USA, 2025.
[17] D. Zenkert, Introduction to Sandwich Construction, Engineering Materials Advisory Services Ltd, 1995.
[18] M.D. McKay, R.J. Beckman, W.J. Conover, A comparison of three methods for selecting values of input variables in the analysis of output from a computer code, Technometrics 21 (2) (1979) 239–245. https://doi.org/10.1080/00401706.1979.10489755
[19] M. Liefvendahl, R. Stocki, A study on algorithms for optimization of Latin hypercubes, J. Stat. Plann. Inference 136 (9) (2006) 3231–3247. https://doi.org/10.1016/j.jspi.2005.01.007
[20] T.W. Simpson, T.M. Mauery, J.J. Korte, F. Mistree, Comparison of response surface and Kriging models for multidisciplinary design optimization, Am. Inst. Aeronaut. Astronaut. 98 (1998) 4755.